ELSEVIER

Journal of Alloys and Compounds 305 (2000) 272–281

Journal of ALLOYS AND COMPOUNDS

www.elsevier.com/locate/jallcom

Hydrogen evolution from Zr-based amorphous and quasicrystalline alloys

N. Eliaz[a,*], D. Eliezer[a], E. Abramov[a], D. Zander[b], U. Köster[b]

[a]*Department of Materials Engineering, Ben-Gurion University of the Negev, Beer-Sheva 84105, Israel*
[b]*Department of Chemical Engineering, University of Dortmund, D-44221 Dortmund, Germany*

Received 3 January 2000; accepted 18 January 2000

Abstract

The combination of local tetrahedral order and favorable chemical composition makes amorphous and quasicrystalline Zr–Cu–Ni–Al alloys good candidates for hydrogen storage applications. Hydrogen evolution from these alloys has been studied by means of thermal desorption spectroscopy (TDS). The characteristics of hydrogen desorption from an initially quasicrystalline phase are analyzed in detail for the first time. Spectra analysis is supported by data from variety of other experimental techniques, such as differential scanning calorimetry (DSC), Auger electron spectroscopy (AES), elastic recoil detection analysis (ERDA) and transmission electron microscopy (TEM). Hydrogen desorption from both alloys is found to be a very complex process, being affected by phase transformations that take place during annealing, by hydride formation, and by the formation of a thin zirconium oxide on the surface.

Keywords: Quasicrystals; Amorphous alloys; Zr-based alloys; Thermal desorption spectroscopy

1. Introduction

The storage capacity of hydrogen in metals and alloys is determined by chemical interactions between the metal and hydrogen atoms, as well as by the type, number and size of the potential interstitial sites for hydrogen. The most common materials for hydrogen storage are metals and alloys that are based on transition metals. In most of these materials, hydrogen tends to occupy tetrahedral interstitial sites. Therefore, the combination of local tetrahedral order and favorable chemical composition makes amorphous and quasicrystalline Zr–Cu–Ni–Al alloys good candidates for hydrogen storage applications. In previous publications [1–6] the authors reported high storage capacity for hydrogen in amorphous and quasicrystalline $Zr_{69.5}Cu_{12}Ni_{11}Al_{7.5}$ alloys. However, hydrogen was observed to exhibit a significant effect not only on the stability of the quasicrystals [1–4,6], but also on their formation from the glassy precursor material [3,5,6]. The objective of this paper is to present results on the characteristics of hydrogen evolution from these alloys. Possible effects of surface barriers, such as zirconium oxide, and of phase transformations that take place during heating of these materials are discussed in detail.

2. Experimental details

Hydrogen evolution from amorphous and quasicrystalline $Zr_{69.5}Cu_{12}Ni_{11}Al_{7.5}$ samples was studied by TDS after electrochemical charging. Amorphous ribbons were prepared by melt spinning. Icosahedral quasicrystals were then formed by annealing above the glass transition temperature, as described elsewhere in detail [7]. Hydrogen charging was carried out electrochemically at room temperature in order to eliminate any possible effects of heating on the metastable materials. Relatively high temperatures (260–300°C) were assumed, for example, to enhance decomposition of Ti–Zr–Ni [8,9] and Zn–Mg–Y [10] quasicrystals to form nanocrystalline hydrides and Laves phases during gaseous charging. Before charging, the samples were ground using 1200-grit paper in order to activate the surface. Charging was carried out in 2:1 (by volume) glycerine: phosphoric acid. Due to the high viscosity of this electrolyte, the mobility of molecular hydrogen in it is relatively small, according to Stokes–

*Corresponding author. Present address: H.H. Uhlig Corrosion Laboratory, Massachusetts Institute of Technology, Cambridge, MA 02139, USA.

0925-8388/00/$ – see front matter
PII: S0925-8388(00)00717-9

Einstein law [11]. The reduced mobility of hydrogen molecules shifts the equilibrium between hydrogen absorption in the sample and hydrogen recombination towards the former [12]. Another advantage of this electrolyte is that it is not too corrosive [13]. However, since this electrolyte is hygroscopic, it should be renewed after several experiments.

The amount of hydrogen absorbed in the material was measured by microbalance with an accuracy of ± 1 μg. Hydrogen content was also measured by ERDA. This technique allows quantifying and depth profiling of hydrogen in thin films. The sample is mounted at a glancing angle with respect to a high-energy (~MeV) ion beam, which causes target atoms to be recoiled from the surface. The energy with which they recoil depends on their mass and on the recoil angle. At known geometries, energy dispersive particle detectors can identify and count the recoiled atoms. Depth profiles are obtained by deconvoluting the energy lost as the ions travel into and exit from the sample surface [14]. This technique has the advantages of being non-destructive and having a resolution of ~1 nm. Volume changes caused by hydrogen absorption were calculated from length changes measured with an inductance strain-gauge device (HBM-W5TK). This sensitive technique, developed by Stolz et al. [15], allows measuring a length change as small as 0.01 μm.

AES was used to study the chemical composition at the surface of the samples before and after hydrogenation. A PHI 549 SAM/AES/XPS system was used. The samples were mounted in a test chamber and a vacuum of $\sim 10^{-10}$ mbar was drawn. Depth profiles were obtained using argon ion sputtering at working conditions ($P \sim 3\times 10^{-5}$ mbar, $i=25$ mA, $V=2$ kV) which yielded a surface removal rate of ~20 Å min^{-1}. Quantitative analysis was based on tables of experimental atomic sensitivity factors [16].

2.1. Thermal desorption spectroscopy (TDS)

Hydrogen desorption was investigated by TDS. Electrochemical charging for these experiments was done in 2:1 glycerine:phosphoric acid-d_3 (D_3PO_4) in order to reduce the background noise. After ultrasonic cleaning in acetone, the sample was placed in a specimen holder, the system was sealed and pumped down to a pressure of $\sim 10^{-8}$ mbar. The desired heating rate and temperature range were programmed on a temperature controller. While heating, the mass spectrometer was placed in a continuous mode for scanning atomic masses in the range 3.5–4.5 amu.

TDS is a very sensitive and accurate technique for studying trapping [17–19] and diffusion [20] processes in crystalline materials. In addition, this technique has been used [21,22] to explore the diffusivity and solubility of hydrogen in amorphous metals. The technique involves accurate measurement of the desorption rate of gas atoms, soluted or trapped in the material, while heating the sample at a known rate. This measurement allows for accurate evaluation of the total quantity of atoms, desorbed within the temperature range of the experiment.

The experimental set-up used in this research is shown in Fig. 1 and has been described in detail elsewhere [17,18,23]. The components of the system were connected by a metallic sealing to allow outgassing of the system and lowering of the gas background, mainly water vapors adsorbed on the chamber walls. A specimen holder, the ionization chamber of the mass spectrometer and a standard deuterium leak for calibration (desorbing gas at a rate of 2.13×10^{-7} atm-cm^3 s^{-1}) were all attached to the UHV chamber. Since the calibration was carried out with a deuterium leak which desorbed gas at a constant rate, the results were not likely to be affected by competition between the rate of desorption from the sample and the system pumping rate, or by partial exchange of desorbed deuterium atoms with hydrogen atoms from the environment to form HD.

The design of the specimen holder is crucial for obtaining reliable and accurate results. First, the material from which it is made should have negligible adsorption, diffusion and solubility coefficients in comparison with the material studied (in order to avoid effects of hydrogen adsorption and desorption from the specimen holder during measurements). Second, the design of the specimen holder should ensure an accurate and uniform temperature profile along the sample. Third, the specimen holder should enable efficient heat transfer to prevent delay in the heating rate of the sample. The specimen holder in this research was cylindrical and made of oxygen-free high copper (OFHC), known for its immunity to hydrogen. A coaxial heating coil surrounded the holder, which allowed fast and accurate heating. The temperature was monitored with a thermocouple located very close to the sample. The temperature controller produced very accurate heating rates, which were typically 3–7°C min^{-1} in this research.

Quantification of several trapping parameters is carried out using the following procedure. When a hydrogenated sample is heated at a constant rate, φ, the rate of hydrogen release from a trap may be described by [22]:

$$\frac{\mathrm{d}c}{\mathrm{d}t} = A(1-c)\exp\left(-\frac{E_{aT}}{RT}\right) \tag{1}$$

where $c=(c_k^o - c_k)/c_k^o$, c_k^o is the amount of hydrogen in the k trapping site at time $t=0$, c_k is the amount of hydrogen in the k trapping site at time $t>0$, A is a reaction rate constant, R is the gas constant, T is the absolute temperature, and E_{aT} is the activation energy for hydrogen release from the trapping site.

This equation represents a first-order desorption, i.e., second-order desorption phenomena such as molecular desorption accompanied by recombination of adsorbed atoms are disregarded. The term $(1-c)$ represents the hydrogen content left in the trap, while $\exp(-E_{aT}/RT)$

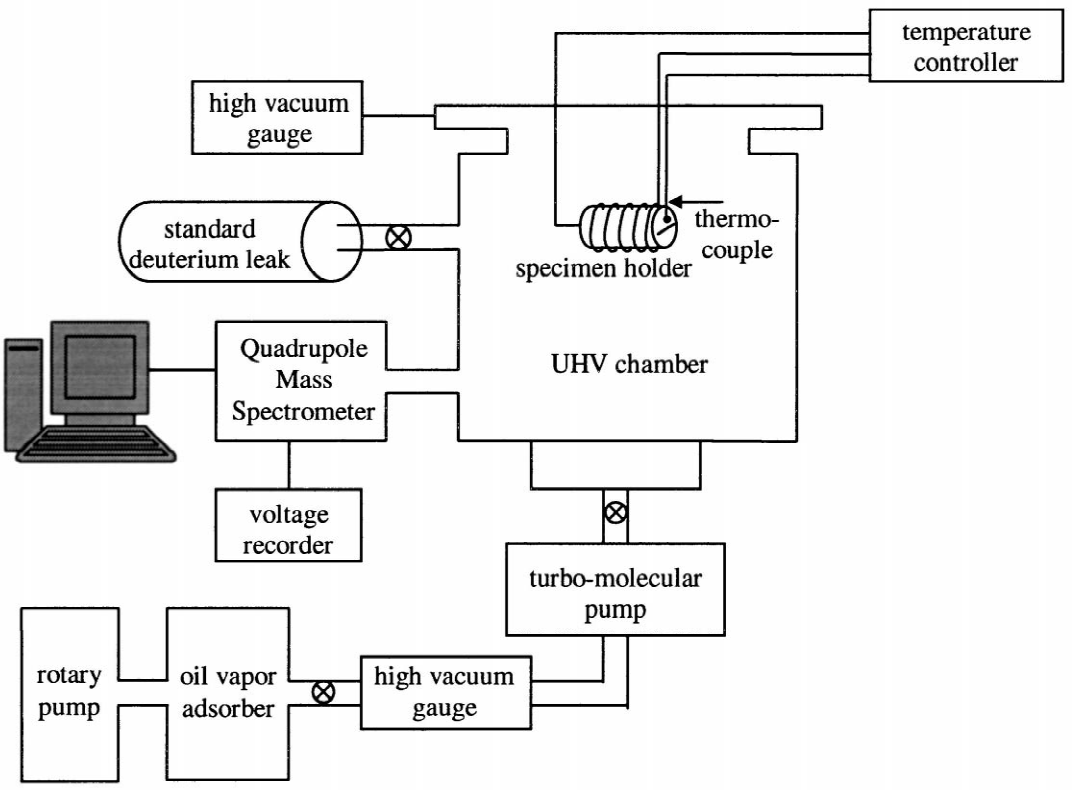

Fig. 1. Schematic view of the apparatus for thermal desorption spectroscopy.

represents the probability for hydrogen release from the trap to a 'normal' interstitial site. When a hydrogenated sample is heated at a constant rate and the rate of hydrogen desorption is plotted versus temperature, a peak is obtained. The desorption rate initially increases since the probability for hydrogen release from a trap increases faster than the decrease in the content of hydrogen in this trap. Subsequently, the desorption rate decreases to zero due to the low hydrogen content remaining in the trap. In general, the temperature producing maximal desorption is determined by the activation energy for hydrogen release from the trap, the order of the desorption reaction and the heating rate. The peak intensity, on the other hand, depends on the content of trapped hydrogen and on the heating rate [24]. Qualitatively, it may be said that the temperature producing maximal desorption reflects the trapping intensity — higher temperature indicates a higher activation energy for hydrogen release. The total amount of gas atoms desorbed during heating characterizes the trap density.

At the maximal hydrogen desorption, the first derivative of Eq. (1) is equal to zero, yielding:

$$\frac{\varphi E_{aT}}{RT_c^2} = A\exp\left[-\frac{E_{aT}}{RT_c}\right] \tag{2}$$

where $T = T_0 + \varphi t$, T_0 is the initial (start) temperature, and T_c is the temperature at the desorption peak.

Eq. (2) may be rewritten as:

$$\ln\left(\frac{\varphi}{T_c^2}\right) = \ln\left(\frac{AR}{E_{aT}}\right) - \frac{E_{aT}}{R}\cdot\frac{1}{T_c} \tag{3}$$

The activation energy for hydrogen release from a trap may be determined graphically by plotting $\ln(\varphi/T_c^2)$ versus $1/T_c$ and calculating the slope of the line. The amount of hydrogen desorbed from the material within the investigated temperature range may be obtained by integrating the plot of desorption rate versus time.

3. Results and discussion

3.1. Hydrogen absorption

On the basis of weight measurements, it has been shown that quasicrystalline $Zr_{69.5}Cu_{12}Ni_{11}Al_{7.5}$ alloy can be electrochemically charged up to a maximum hydrogen content of 1.6 H/M before failure of the ribbon initiates [2]. This content is high in comparison with the maximum hydrogen content of 1.0 H/M attainable in the counterpart amorphous alloy [3], as well as in comparison with the capacities of many typical systems used in hydrogen storage applications [25,26]. The hydrogen content, as measured by weight measurements, is supported by both the calculation of a typical [25,27] molar volume of 2.4×

10^{-3} nm^3/H-atom in the amorphous alloy [5] and ERDA experiments [4]. The latter also revealed that the hydrogen concentration decreases significantly in a thin layer just beneath the surface.

The storage capacity was found to be larger and the absorption kinetics faster for the quasicrystalline phase than for the counterpart amorphous one [3]. This improved storage capacity may result from the large number of adjacent tetrahedral sites in the icosahedral structure (20 tetrahedra in each icosahedron). The faster absorption kinetics is more difficult to explain, as the characteristics of defects in the quasicrystalline structure and the location of different kinds of atoms in the icosahedron are not known. Qualitatively, however, if hydrogen transport is dominated by hopping, the large number of adjacent tetrahedral sites in the quasicrystalline structure may also explain the faster kinetics. Another possibility would be that the defects present in the quasicrystalline structure act as short-circuit paths for hydrogen diffusion.

3.2. Hydrogen evolution

In this part, the desorption of deuterium from the amorphous and quasicrystalline alloys is discussed. As will be shown, the total amount of deuterium desorbed from these alloys within the temperature range of investigation is much smaller than the content obtained by weight measurements. Therefore, interpretation of the TDS spectra should be made very carefully.

Figs. 2 and 3 show the variation of thermal desorption (TD) from the quasicrystalline and amorphous alloys, respectively, with charging time. A typical dependence of TD from the amorphous alloy on the heating rate is shown in Fig. 4. Table 1 summarizes some major parameters of hydrogen charging and TDS experiments, from which the spectra presented in Figs. 2–4 as well as some other spectra were obtained. This table also summarizes the values of several parameters characterizing the desorption of hydrogen from the amorphous and quasicrystalline alloys. Comparing the desorption profiles with DSC plots of the as-cast as well as hydrogenated amorphous and quasicrystalline alloys, it is apparent that most of the hydrogen has not desorbed prior to the formation or decomposition of the quasicrystalline phase (which take place within the temperature range 400–500°C). This made it very easy to investigate the influence of hydrogen on the formation and decomposition of the quasicrystalline phase [3–6].

As shown in Figs. 2 and 3 for an identical heating rate, deuterium desorption from the amorphous alloy starts and ends at lower temperatures in comparison with desorption from the quasicrystalline alloy. This behavior may result from either higher activation energy for detrapping or the existence of stronger surface barriers in the quasicrystalline alloy. In addition, phase transformations may allow deuterium release. In such a case, desorption from the initially amorphous alloy can be expected to start at lower temperatures, as the temperature for the formation of quasicrystals is lower than that of their decomposition.

A second difference between the desorption profiles for the amorphous and quasicrystalline alloys is evident. As charging time increases, the main desorption peak of the amorphous alloy is shifted to lower temperatures, while that of the quasicrystalline alloy is shifted to higher temperatures. In general, such a shift as for the amorphous alloy is often explained in terms of occupancy of sites of

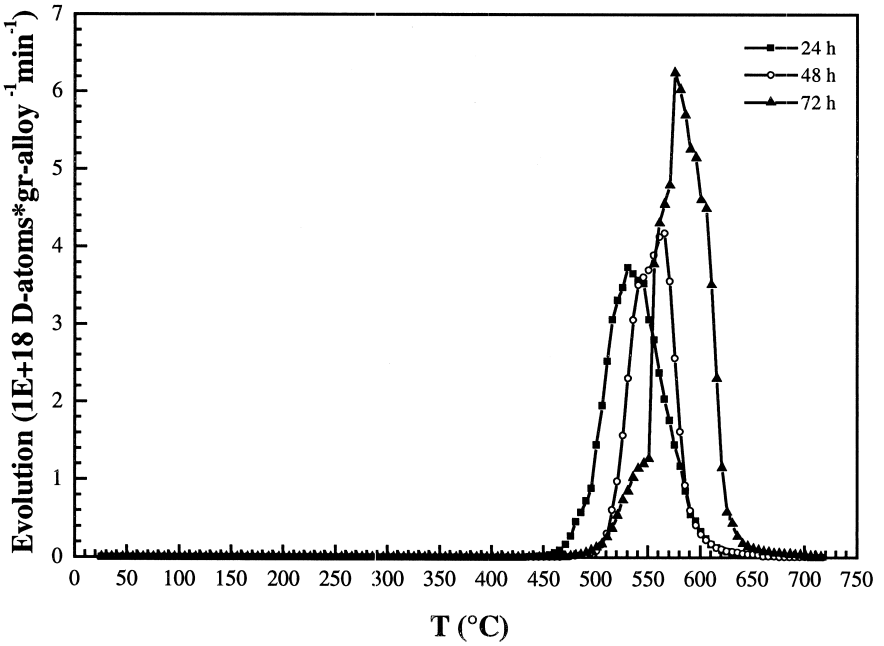

Fig. 2. Variation with charging time of deuterium evolution from quasicrystalline $Zr_{69.5}Cu_{12}Ni_{11}Al_{7.5}$ charged at $i = 10$ A m^{-2}. Heating rate, 5°C min^{-1}.

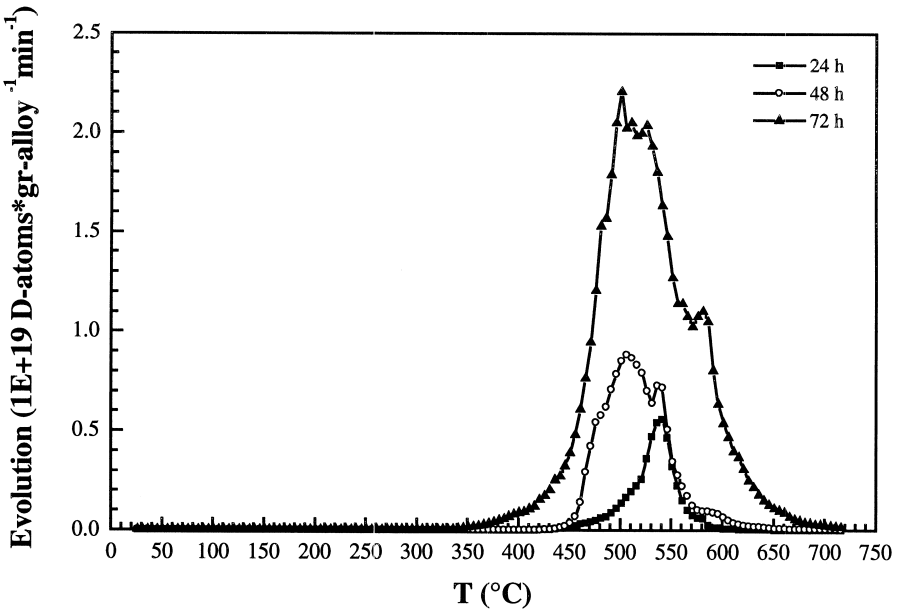

Fig. 3. Variation with charging time of deuterium evolution from amorphous $Zr_{69.5}Cu_{12}Ni_{11}Al_{7.5}$ charged at $i=10$ A m^{-2}. Heating rate, 5°C min^{-1}.

shallower energy levels in the amorphous structure [21,28]. However, since phase transformations in the Zr–Cu–Ni–Al system take place in parallel to desorption, it is more reasonable to relate the desorption peak to deuterium released during the decomposition of quasicrystals (whose temperature decreases as hydrogen content increases — according to DSC results [3]). The shift of the desorption peak in the case of the initially quasicrystalline alloy may be explained in terms of random occupation of new traps with different energy levels and/or formation of surface barriers to desorption during cathodic charging.

Several other differences are apparent when comparing the TDS plots of the amorphous and quasicrystalline alloys. The main desorption peak for the quasicrystalline alloy is narrower than the equivalent peak for the amorphous alloy. This narrowing may be related to reordering

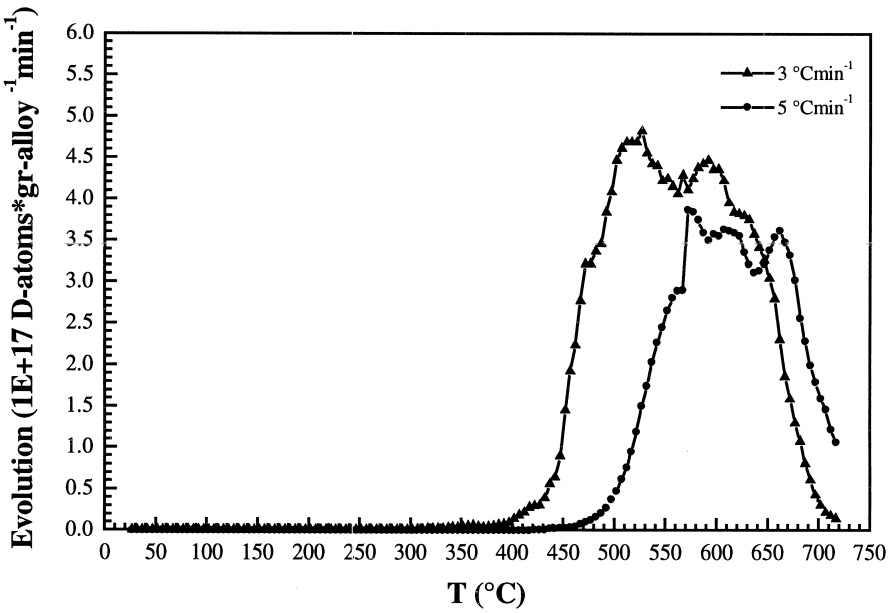

Fig. 4. Temperature ramp dependence of deuterium evolution from amorphous $Zr_{69.5}Cu_{12}Ni_{11}Al_{7.5}$ charged at $i=100$ A m^{-2}. Charging time, 4 h.

Table 1
Experimental conditions of hydrogen charging and thermal desorption experiments, as well as values of trapping parameters extracted from the TDS spectra of amorphous and quasicrystalline $Zr_{69.5}Cu_{12}Ni_{11}Al_{7.5}$ alloys

Material	Charging conditions i (A m^{-2}), t (h)	Heating rate φ (°C min^{-1})	Temp. at desorption peak T_c (°C)	Maximal desorption rate (atoms s^{-1})	Amount desorbed (H/M)
Quasicrystalline alloy	$t=24$, $i=10$	5	531	5.01×10^{14}	6.78×10^{-3}
	$t=48$, $i=10$	5	564	4.38×10^{14}	5.67×10^{-3}
	$t=72$, $i=10$	5	579	6.96×10^{14}	9.51×10^{-3}
	$t=24$, $i=10$	3	469	2.59×10^{14}	3.00×10^{-3}
	$t=24$, $i=10$	7	548	9.84×10^{14}	7.89×10^{-3}
Amorphous alloy	$t=24$, $i=10$	5	542	9.36×10^{14}	6.57×10^{-3}
	$t=48$, $i=10$	5	506	1.43×10^{15}	1.82×10^{-2}
			538	1.17×10^{15}	
	$t=72$, $i=10$	5	501	8.88×10^{15}	6.15×10^{-2}
			524	8.19×10^{15}	
			580	4.44×10^{15}	
	$t=48$, $i=10$	7	566	2.93×10^{15}	2.48×10^{-2}
	$t=4$, $i=100$	3	527	1.61×10^{14}	–[a]
			567	1.43×10^{14}	
			592	1.49×10^{14}	
	$t=4$, $i=100$	5	577	7.07×10^{13}	–[a]
			607	6.65×10^{13}	
			663	6.61×10^{13}	

[a] Total amount of desorbed deuterium is not shown since cathodic charging was conducted at a different experimental set-up.

of the atoms, accompanied by elimination of free volume and decrease in the mean size of interatomic spacing during heat treatment to form the quasicrystalline phase in the amorphous matrix. Such a phenomenon was reported, for example, after annealing of amorphous $Pd_{80}Si_{20}$ [22]. The wider peak of the initially amorphous alloy, however, may also result from the existence of a temperature range between the formation and decomposition of quasicrystals, within which desorption is enhanced. This range does not exist in the case of the initially quasicrystalline alloy. In the case of the quasicrystalline alloy (Fig. 2), the desorption peak is not shifted to lower temperatures and its width almost does not increase as charging time increases. Thus, models of continuous distribution of site energies (as those suggested by Kirchheim [29,30] for amorphous alloys) are not applicable to the quasicrystalline structure. Moreover, using the equations developed by Carter [24] to describe the initial site occupancy in the case of a single activation energy and first- or second-order desorption, the hydrogen content in the quasicrystalline alloy was found to be about one order of magnitude higher than that obtained by integration of the experimental plot. Therefore, models of single activation energy and first- or second-order desorption are also not applicable to the evolution of hydrogen from the quasicrystalline alloy.

Apparently, deuterium desorption from the quasicrystalline alloy is characterized by a single peak. Taking into account the shift of this peak at different heating rates, the effective activation energy for deuterium release is calculated using Eq. (3) to be: $E_{aT}=0.39\pm0.06$ eV atom^{-1}. However, a careful examination indicates that this peak may be a superposition of at least two or three smaller peaks (see, for example, sharp changes in the slope of the plot related to 72 h of charging at 551 and 571°C).

In the case of the amorphous alloy, several distinct desorption peaks appear, especially as charging time (Fig. 3) or charging current density increase (for the latter compare between the spectrum in Fig. 4 corresponding to 5°C min^{-1} and Fig. 3). It is well known that in the zirconium–hydrogen system, hydrides of different chemical compositions and crystalline structures may form [25]. Therefore, different desorption peaks may be related to decomposition of specific hydrides. However, on the basis of TEM, DSC and XRD results [3,5,6] it is more likely that the various peaks result from deuterium release during phase transformations and from microstructures, which become more complex as the initial hydrogen content increases.

The total deuterium content (3.00×10^{-3}–9.51×10^{-3} H/M) measured during thermal desorption from the quasicrystalline alloy is more than two orders of magnitude lower than the content obtained by weight measurements. In addition, deuterium content as measured by TD does not change significantly when charging time increases. Such discrepancies may be explained by the results of TEM studies that were performed by the authors and reported recently [6]. These results indicate that at very high hydrogen concentrations (H/M>1.1), decomposition of quasicrystals starts with the precipitation of tetragonal ZrH_{2-x}. As the lattice parameters of the stable ε-hydride

strongly depend on the hydrogen content [31], it could be concluded that the composition of the hydride which is formed during decomposition of the hydrogenated quasicrystals corresponds to H/Zr~1.6. This value is in good agreement with the measured hydrogen content after charging, as well as with the small amount of deuterium that was desorbed around 500°C. In-depth studies of this hydride formation are in progress.

3.3. Role of oxide film

The latter discrepancies may also result from the formation of an oxide layer, which hinders hydrogen desorption, on the surface. For the amorphous alloy, the total amount of deuterium (6.57×10^{-3}–6.15×10^{-2} H/M) measured during TD is more than one order of magnitude smaller than the hydrogen content obtained by weight measurements. In this case, however, the difference between TDS and weight measurement results is much smaller, and the total amount of deuterium changes significantly as charging time increases. Thus, a thicker and more uniform oxide (ZrO_2) layer may form on the surface of the quasicrystalline alloy. Faster kinetics of oxide formation in the case of the quasicrystalline alloy may result, for instance, from higher diffusivity of zirconium in the quasicrystalline structure. This layer, formed during or shortly after electrochemical charging, serves as a barrier to hydrogen desorption from the alloy. Since the bonds in this oxide are ionic, it cannot dissolve hydrogen, which is supported by the ERDA results aforementioned. Since this layer is very thin, however, its formation almost does not affect the results of weight measurements. Additional evidence of the role of surface barriers arises from another series of TDS experiments. In these experiments it was found that the total amount of desorbed hydrogen depends on the level of surface preparation (grinding) of the quasicrystalline ribbon before electrochemical charging.

In order to determine whether oxide layer exists on the surface of the charged samples and whether its thickness depends on the microstructure of the material and/or on charging time, several samples were studied by AES. Fig. 5 shows Auger spectra after (a) 1 min and (b) 4 min of sputtering for three different samples: ground quasicrystalline ribbon; amorphous ribbon ground and electrochemically charged for 72 h at 10 A m^{-2}; and quasicrystalline ribbon ground and charged under identical conditions. The energy range in the figure was chosen to emphasize the formation of ZrO_2, thus the spectra do not include peaks of copper and nickel (which were identified at higher energies). Zirconium is characterized by five major peaks at energies of 92 (related to $M_5N_1N_{2,3}$ transition), 116 ($M_5N_{2,3}N_{2,3}$), 128 (M_4N_2V), 147 ($M_4N_{2,3}N_{4,5}$) and 174 eV ($M_5N_{4,5}N_{4,5}$). Oxygen has three peaks at 475 (KL_1L_1), 490 (KL_1L_2) and 510 eV (KL_2L_2). After a minute of sputtering, the amplitude of the peak O_{510} is larger than the amplitudes of the zirconium peaks in all three samples. In addition, the shape of the peaks in the charged quasicrystalline alloy is slightly different from the uncharged sample (see, for example, the splitting to two of the Zr_{147} peak in the charged sample). After 4 min of sputtering, the ratio between the amplitudes of the zirconium peaks and the amplitude of the oxygen peaks increases, and the shape of the former becomes similar to that of zirconium in the metallic chemical state. In addition, the ratio between the amplitude of the Zr_{147} peak and the amplitude of the Zr_{92} peak increases. This results from the fact that the former is related to valance electrons, while the latter is related to core electrons (and, thus, less affected by the chemical environment). Thus, comparing the spectra shown in Fig. 5 with Auger spectra of zirconium and zirconium oxide reported elsewhere [16,32–34], it may be concluded that all samples are oxidized at the surface, and that the level of oxidation increases after cathodic charging.

Fig. 6 shows the sputtering time dependence of the atomic fraction of zirconium and oxygen on the surfaces of the three samples. Calculations were made on the basis of the Zr_{147} and O_{510} peaks, using atomic sensitivity factors of 0.22 and 0.5, respectively [16]. Since the amplitudes of the other peaks (C, Ca, Ar, Cu, Ni, Al) are not taken into account, these calculations should be treated only as a comparative measure of the oxidation level at the surface. It can be seen that as the sputtering time increases, the oxygen content decreases and the zirconium content increases. In addition, the respective rates increase from the charged quasicrystalline sample, to the charged amorphous sample, and finally to the uncharged quasicrystalline sample. Examining the change in the shape of the depth profiles, the thickness of the oxide layer may be estimated to be about 3.3 nm in the uncharged quasicrystalline sample, about 4 nm in the charged amorphous sample, and about 8 nm in the charged quasicrystalline sample.

In order to reduce the effect of the zirconium oxide on hydrogen evolution, three different techniques have been explored. By the first technique, the sample was reground just before its introduction into the vacuum chamber. However, an even smaller content of deuterium was measured in this experiment, probably due to removal of material that contained deuterium together with the removal of oxide. By the second technique, the samples were coated with palladium before charging by means of chemical deposition or thermal evaporation. However, in both cases satisfactory adhesion between the sample and the coating could not be attained. By the third technique, the amorphous alloy was alloyed with palladium (up to $Zr_{68.5}Cu_{13}Pd_{11}Al_{7.5}$). Consequently, faster hydrogen absorption kinetics was obtained, probably due to segregation of palladium to the surface of the sample. However, since such palladium additions prevent the formation of quasicrystals, this technique was not further used. Other techniques for overcoming the problem of oxide formation are currently being studied. It should be noted that until

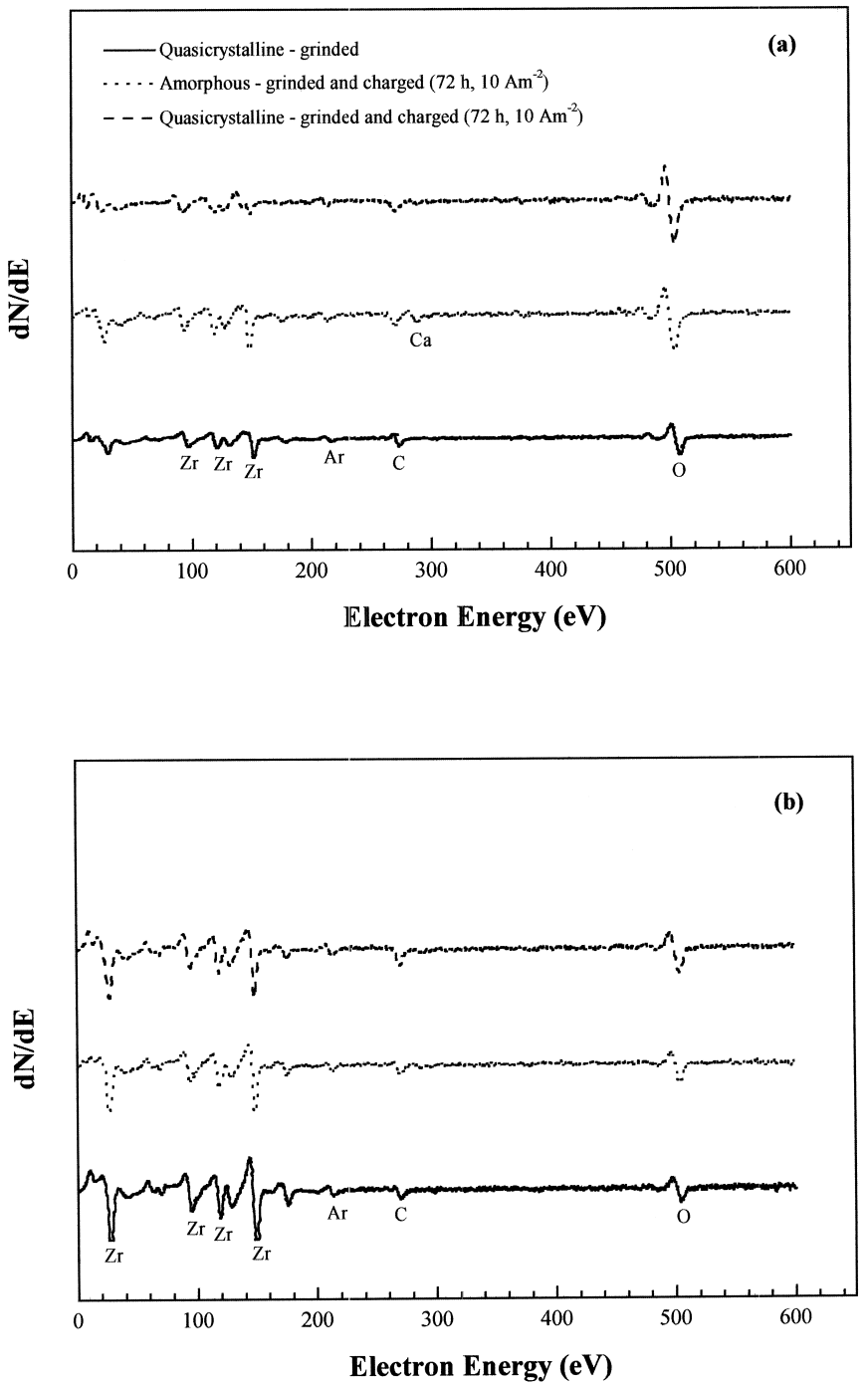

Fig. 5. AES spectra from the surface region of Zr–Cu–Ni–Al ribbons after (a) 1 min and (b) 4 min of sputtering with Ar ions.

hydrogen evolution from these materials is significantly improved, they cannot be used for hydrogen storage applications. In addition to developing techniques to activate the hydrogenated alloy, one may consider modifications in the chemical composition of the alloy. Such modifications, for example, have recently led to the observation of a plateau in the pressure–concentration–isotherms (P–C–T) of amorphous $Zr_{55}Al_{10}Ni_5Cu_{30}$ alloy for which the temperature region between the glass and crystallization temperatures is rather large [35].

4. Conclusions

Hydrogen evolution from amorphous and quasicrystalline Zr–Cu–Ni–Al alloys was studied in the framework of

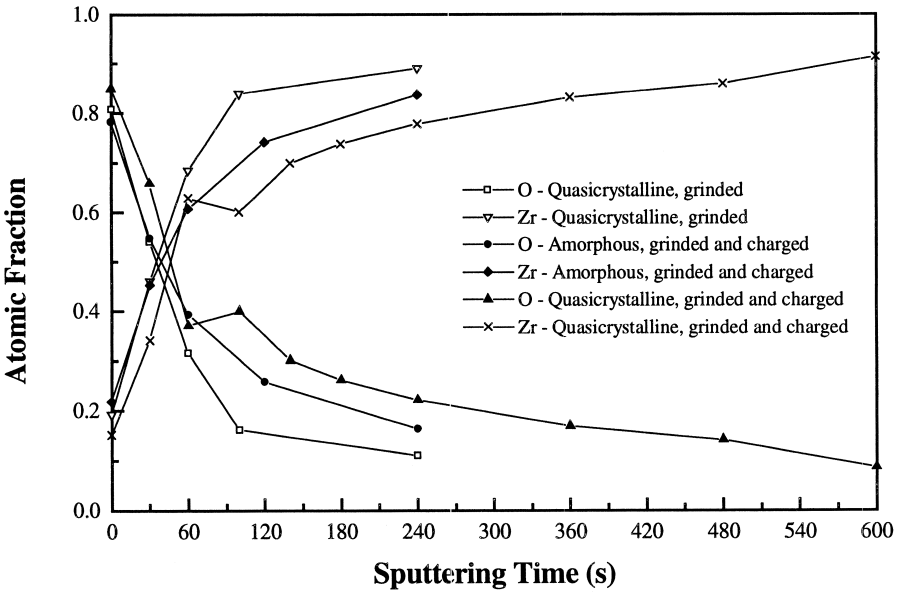

Fig. 6. Depth profiles of the atomic fraction of Zr and O, calculated from AES spectra.

evaluating the applicability of these materials to hydrogen storage devices. For the first time, the characteristics of hydrogen desorption from an initially quasicrystalline phase were analyzed in detail. Desorption of hydrogen from these materials was found to be a very complex process affected by:

1. phase transformations that take place in parallel to the desorption process;
2. the dependence of the microstructures, which are formed during annealing, on the initial hydrogen content in the alloy;
3. a very thin layer of ZrO_2 (several nanometers in thickness), formed during or just after electrochemical charging;
4. hydride formation during decomposition of the hydrogenated quasicrystals.

The small amount of hydrogen desorbed from these materials at temperatures as high as 700°C prevents the current use of either amorphous or quasicrystalline $Zr_{69.5}Cu_{12}Ni_{11}Al_{7.5}$ alloys for hydrogen storage applications. Ways of activating the hydrogenated alloy and compositional modifications are considered to overcome this problem.

Acknowledgements

This work was partially supported by the Deutsche Forschungsgemeinschaft (DFG Ko 668/22) and the German–Israel Foundation for Scientific Research and Development (GIF I-531-046.10/97). The authors would like to thank Dr D. Plachke from MPI für Metallforschung in Stuttgart for running the ERDA experiments. The assistance of Dr N. Froumin from Ben-Gurion University in AES experiments is highly appreciated.

References

[1] B.I. Wehner, J. Meinhardt, U. Köster, H. Alves, N. Eliaz, D. Eliezer, Mater. Sci. Eng. A 226–228 (1997) 1008.
[2] U. Köster, D. Zander, J. Meinhardt, N. Eliaz, D. Eliezer, in: S. Takeuchi, T. Fujiwara (Eds.), Proc. 6th Int. Conf. on Quasicrystals — ICQ6, World Scientific, Singapore, 1998, p. 313.
[3] D. Zander, H. Leptien, U. Köster, N. Eliaz, D. Eliezer, J. Non-Cryst. Solids 250–252 (1999) 893.
[4] D. Zander, U. Köster, N. Eliaz, D. Eliezer, D. Plachke, in: J.-M. Dubois, P.A. Thiel, A.-P. Tsai, K. Urban (Eds.), Materials Research Society Symp. Proc. 1998, Quasicrystals, Vol. 553, MRS, Pennsylvania, 1999, p. 49.
[5] U. Köster, D. Zander, H. Leptien, N. Eliaz, D. Eliezer, in: W.L. Johnson, C.T. Liu, A. Inoue (Eds.), Materials Research Society Symp. Proc. 1998, Bulk Metallic Glasses, Vol. 554, MRS, Pennsylvania, 1999, p. 287.
[6] D. Zander, U. Köster, N. Eliaz, D. Eliezer, Influence of hydrogen on formation and stability of Zr-based quasicrystals, Mater. Sci. Eng. A, in press.
[7] U. Köster, J. Meinhardt, S. Roos, H. Liebertz, Appl. Phys. Lett. 69 (1996) 179.
[8] A.M. Viano, R.M. Stroud, P.C. Gibbons, A.F. McDowell, M.S. Conradi, K.F. Kelton, Phys. Rev. B 51 (17) (1995) 12026.
[9] A.M. Viano, A.F. McDowell, M.S. Conradi, P.C. Gibbons, K.F. Kelton, in: C. Janot, R. Mosseri (Eds.), Proc. 5th Int. Conf. on Quasicrystals, World Scientific, Singapore, 1995, p. 798.
[10] A.P. Tsai, A. Niikura, A. Inoue, T. Masumoto, in: C. Janot, R. Mosseri (Eds.), Proc. 5th Int. Conf. on Quasicrystals, World Scientific, Singapore, 1995, p. 628.
[11] J.O'M. Bockris, A.K.N. Reddy, Modern Electrochemistry, Vol. 1, Plenum Press, New York, 1970, pp. 379, 550.
[12] R. Kirchheim, R.B. McLellan, J. Electrochem. Soc. 127 (1980) 2419.

[13] D. Menzel, A. Niklas, U. Köster, Mater. Sci. Eng. A 133 (1991) 312.
[14] http://www.rmcs.cranfield.ac.uk/departments/dmms/cranan/erda.shtml
[15] U. Stolz, U. Nagorny, R. Kirchheim, Scripta Metall. 18 (1984) 347.
[16] L.E. Davis, C.N. MacDonald, P.W. Palmberg, G.E. Riach, R.E. Werber, in: Handbook of Auger Electron Spectroscopy, Perkin Elmer, Eden Prairie, MN, 1978.
[17] E. Abramov, D. Eliezer, in: A.W. Thompson, N.R. Moody (Eds.), Proc. 5th Int. Conf. on the Effect of Hydrogen on the Behavior of Materials, TMS, 1996, p. 293.
[18] E. Abramov, D. Eliezer, Metall. Trans. A 25 (1994) 949.
[19] K.L. Wilson, M.I. Baskes, J. Nucl. Mater. 76/77 (1978) 291.
[20] G. Farrel, G. Carter, Vacuum 17 (1967) 15.
[21] J.B. Han, D.W. Kweon, J.-Y. Lee, J. Non-Cryst. Solids 108 (1989) 216.
[22] S.-M. Lee, J.-Y. Lee, J. Appl. Phys. 63 (9) (1988) 4758.
[23] N. Eliaz, Hydrogen Interaction with Amorphous and Quasicrystalline Alloys, Ph.D. Thesis, Ben-Gurion University of the Negev, Israel, June, 1999.
[24] G. Carter, Vacuum 12 (1962) 245.
[25] Y. Fukai, The Metal–Hydrogen System, Materials Science, Vol. 21, Springer-Verlag, Berlin, 1993.
[26] R.G. Barnes (Ed.), Hydrogen storage materials (Materials Science Forum, Vol. 31), Trans. Tech. Publications, Switzerland, 1988.
[27] A.J. Maeland, in: S. Steeb, H. Warlimont (Eds.), Rapidly Quenched Metals, Elsevier, Amsterdam, 1985, p. 1507.
[28] R. Kirchheim, F. Sommer, G. Schluckebier, Acta Metall. 30 (1982) 1059.
[29] R. Kirchheim, Acta Metall. 30 (1982) 1069.
[30] R. Kirchheim, Acta Metall. 21 (1973) 1233.
[31] H.J. Goldschmidt, in: Interstitial Alloys, Butterworth, London, 1967, p. 477.
[32] L.R. Danielson, J. Vac. Sci. Technol. 20 (1) (1982) 86.
[33] G.N. Krishnan, B.J. Wood, D. Cubicciotti, J. Electrochem. Soc. 128 (1) (1981) 191.
[34] R. Sherman, J. Mater. Sci. Lett. 3 (1984) 711.
[35] T. Shoji, A. Inoue, J. Alloys Comp. 292 (1999) 275.